SCRIB expression is deregulated in human prostate cancer, and its deficiency in mice promotes prostate neoplasia

Helen B. Pearson,[1] Pedro A. Perez-Mancera,[2] Lukas E. Dow,[1,3] Andrew Ryan,[4] Pierre Tennstedt,[5] Debora Bogani,[6] Imogen Elsum,[1,7] Andy Greenfield,[6] David A. Tuveson,[2] Ronald Simon,[5] and Patrick O. Humbert[1,7,8]

[1]Cell Cycle and Cancer Genetics Laboratory, Peter MacCallum Cancer Centre, East Melbourne, Victoria, Australia. [2]Tumor Modelling and Experimental Medicine (Pancreatic Cancer), Cancer Research UK, Cambridge Research Institute, Li Ka Shing Centre, Cambridge, United Kingdom. [3]Cold Spring Harbor Laboratory, Cold Spring Harbor, New York, USA. [4]TissuPath, Mount Waverley, Victoria, Australia. [5]Institute of Pathology, University Medical Centre Hamburg-Eppendorf, Hamburg, Germany. [6]Mammalian Genetics Unit, Medical Research Council Harwell, Oxford, United Kingdom. [7]Department of Molecular Biology and Biochemistry and [8]Department of Pathology, University of Melbourne, Parkville, Victoria, Australia.

Loss of cellular polarity is a hallmark of epithelial cancers, raising the possibility that regulators of polarity have a role in suppressing tumorigenesis. The Scribble complex is one of at least three interacting protein complexes that have a critical role in establishing and maintaining epithelial polarity. In human colorectal, breast, and endometrial cancers, expression of the Scribble complex member SCRIB is often mislocalized and deregulated. Here, we report that Scrib is indispensable for prostate homeostasis in mice. *Scrib* heterozygosity initiated prostate hyperplasia, while targeted biallelic *Scrib* loss predisposed mice to prostate intraepithelial neoplasia. Mechanistically, Scrib was shown to negatively regulate the MAPK cascade to suppress tumorigenesis. Further analysis revealed that prostate-specific loss of Scrib in mice combined with expression of an oncogenic *Kras* mutation promoted the progression of prostate cancer that recapitulated the human disease. The clinical significance of the work in mice was highlighted by our observation that SCRIB deregulation strongly correlated with poor survival in human prostate cancer. These data suggest that the polarity network could provide a new avenue for therapeutic intervention.

Introduction

Distinct functional and spatial domains are created within epithelial cells owing to the unequal distribution of cellular constituents, referred to as cellular polarity (1). The spatial asymmetry of polarity regulators permits epithelial cells to respond to extracellular cues and maintains the tissue architecture and cellular polarity required for normal physiological function and tissue homeostasis (2, 3). Loss of cell and tissue polarity is a frequent characteristic of epithelial cancers, suggesting a crucial role for polarity mediators in suppressing tumorigenesis (2, 4).

The mammalian polarity program is established by at least three interacting protein complexes (Scrib, Crumbs, and Par) and mediates a plethora of polarization processes, including apical-basal polarity, migration, asymmetric cell division, and planar cell polarity (2, 3). The apical protein modules termed the Crumbs (Pals, PatJ, and Crumbs) and Par (Par3, Par6, and aPKC) complexes act in a mutually antagonistic relationship with the basolateral Scribble module (5). The Scribble module comprises Scrib, Discs large 1–4 (Dlg1–4), and lethal giant larvae 1/2 (Lgl1/2) (5). Together, these complexes mediate a complex series of processes to establish and maintain polarity, including the formation of cell-cell contacts (i.e., adherens and tight junction assembly) (3).

Scrib was originally identified as a neoplastic tumor suppressor in *Drosophila* (6), whereas human SCRIB was discovered as a target for ubiquitin-mediated degradation by the human papillomavirus (HPV) E6 proteins and E6AP protein ligase (7), which also target human DLG1 (8). Cervical carcinomas are commonly associated with HPV and have been shown to display reduced SCRIB and DLG1 protein expression (9, 10).

Deregulation of Scribble complex members (SCRIB, DLG1, and LLGL2) has been correlated to a number of human epithelial cancers (11–14), although somatic mutations remain to be identified. Human colorectal, breast, and endometrial cancers display mislocalized and deregulated SCRIB expression (14–18), suggesting that SCRIB may be crucial for the homeostatic maintenance of several epithelial tissues. Together, these data highlight the critical function of the Scribble module to maintain epithelial tissue architecture and cellular polarity to prevent tumor onset and progression.

SCRIB has been implicated in the regulation of many cellular processes, including proliferation, differentiation, apoptosis, stem cell maintenance, migration, vesicle trafficking, and apical-basal polarity (5). These events appear to be mediated through several emerging oncogenic signaling cascades, such as the Ras/MAPK, β-catenin/Wnt, planar cell polarity, and Notch pathways, indicating direct mechanisms whereby SCRIB could suppress tumorigenesis (5). SCRIB encodes a large, 220-kDa cytoplasmic scaffolding protein that comprises a large leucine-rich repeat (LRR) region and 4 PDZ domains that regulate protein-protein interactions (5, 7), including SCRIB-LLGL2 (19). Other reported SCRIB binding partners include the tight junction protein ZO-2 (20), the planar cell polarity protein VANGL2 (19), the tumor suppressor adenomatous polyposis coli (APC) (21), and the MAPK signaling molecule ERK (22). In fact, previous in vitro work undertaken in our labora-

Conflict of interest: The authors have declared that no conflict of interest exists.
Citation for this article: *J Clin Invest.* 2011;121(11):4257–4267. doi:10.1172/JCI58509.

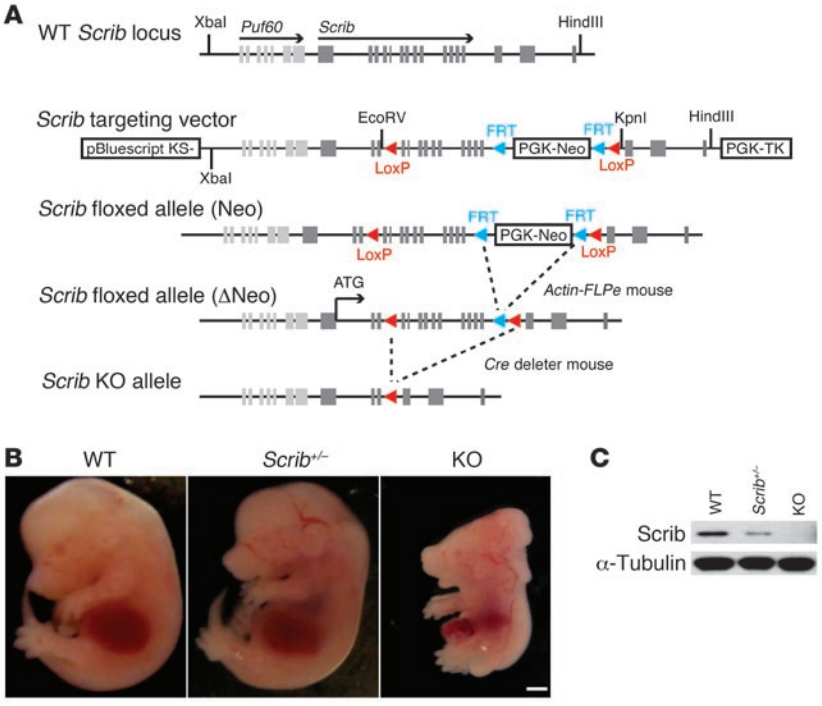

Figure 1
Generation and analysis of *Scrib*-deficient mice. (**A**) Schematic representation of the WT *Scrib* allele, targeting construct, and mutated *Scrib* allele. Excision of the Frt-flanked PGK-Neo cassette in the LoxP-flanked targeting vector was accomplished by crossing $Scrib^{fl\text{-}Neo}$ mice to *Actin-FLPe* mice, producing the *Scrib* floxed ($Scrib^{fl}$) allele. The insertion of EcoRV and KpnI restriction sites permitted screening for recombinant ES cell clones (see Supplemental Figure 1, A and B). *Scrib*-KO mice were derived by crossing $Scrib^{+/fl}$ mice with a germline *Cre*-deleter mouse. Exons are indicated as boxes and LoxP/FLPe sites as triangles. (**B**) Photographs of WT, $Scrib^{+/-}$, and KO E14.5 embryos. Scale bar: 10 mm. (**C**) Western blot analysis of embryonic brain lysates (E16.5) confirmed Scrib loss in $Scrib^{+/-}$ and KO compared with WT embryos.

tory and others has indicated that SCRIB may negatively regulate the RAS/MAPK cascade to maintain polarity and tissue homeostasis (22, 23). Furthermore, studies in *Drosophila* and mammalian cell lines show that SCRIB loss and RAS activation cooperate to promote invasion (23, 24).

Despite these striking human cancer associations and biochemical and functional findings, the tumor-suppressive role of Scrib remains to be determined in vivo. To directly assess this possibility, we generated and characterized global and tissue-specific Scrib–deficient mice. We show that prostate homeostasis is highly sensitive to Scrib deregulation and demonstrate that *Scrib* heterozygosity is sufficient to cause focal prostate hyperplasia, whereas biallelic loss within prostate epithelium promoted disease progression to low-grade prostate intraepithelial neoplasia (LG-PIN). We observed loss of cellular polarity and elevated proliferation concomitant with elevated Ras/MAPK signaling in Scrib-deficient prostate lesions, suggesting that Scrib negatively regulates the Ras/MAPK cascade to suppress prostate tumorigenesis. In support of this notion, chemical inhibition of the Ras/MAPK cascade demonstrated that this pathway is required for hyperplastic growth in the context of Scrib deficiency. Additionally, we reveal that Scrib loss and oncogenic K-ras cooperate to promote prostate cancer progression using the $PBCre^{+}$ transgenic line to drive Scrib depletion and expression of oncogenic K-ras ($LSL\text{-}K\text{-}ras^{G12D}$) specifically within the prostate. This compound transgenic model recapitulates key pathophysiological aspects of the human disease and exemplifies the tumor-suppressive function of Scrib during prostate cancer initiation and progression. Importantly, we determine that SCRIB is deregulated in human prostate cancer and that aberrant SCRIB localization strongly correlates with poor survival. These studies establish Scrib as a critical barrier to prostate tumorigenesis and present polarity proteins as potential prognostic markers in the clinic.

Results

Generation of Scrib conditional knockout mouse. To test whether deregulation of Scrib expression predisposes to epithelial cancer in vivo, we engineered mice harboring a conditional knockout allele of the *Scrib* gene (Figure 1A and Supplemental Figure 1, A and B; supplemental material available online with this article; doi:10.1172/JCI58509DS1). *Cre* recombinase expression results in the excision of exons 4–13, comprising the majority of the LRR domain, which is required for Scrib function (16, 25, 26). This deletion introduces a nonsense mutation in the nascent *Scrib* mRNA and a frameshift in the translation reading frame, predicted to produce a small protein fragment (100 aa) with no known functional domains.

To examine the effect of ubiquitous Scrib deficiency, we crossed mice harboring a LoxP-flanked *Scrib* allele ($Scrib^{+/fl}$) to a germline *Cre*-deleter transgenic line (27), resulting in viable $Scrib^{+/-}$ progeny. To engineer global depletion of Scrib (KO), we intercrossed $Scrib^{+/-}$ mice. Genotyping of embryos confirmed normal Mendelian ratios, yet *Scrib*-KO mice died perinatally owing to a severe neural tube closure defect (craniorachischisis) (Figure 1B and Supplemental Figure 1C). All KO embryos displayed a curly tail, eyes open at birth, and gonad morphological abnormalities of both sexes, and 54% (14 of 26) displayed defective abdominal wall closure (gastroschisis) (Supplemental Figure 1, D–F). These characteristics mirror the *Circletail* (*Crc*) and *rumz* Scrib point mutation models, consistent with specific ablation of *Scrib* gene function (28, 29). Western blot analysis confirmed that Scrib was efficiently depleted in vivo, indicating the *Scrib*-KO allele is a true null allele (Figure 1C).

$Scrib^{+/-}$ mice display prostate hyperplasia. Loss of polarity has been implicated as a hallmark of epithelial cancers (4); however, it remains to be determined whether deregulation of polarity regulators is a tumor-initiating event or a consequence of transformation. To address whether reduced Scrib expression is sufficient to drive epithelial tumorigenesis, we initially examined epithelial tissues from a cohort of $Scrib^{+/-}$ mice at 100 days of age (n = 10). Remark-

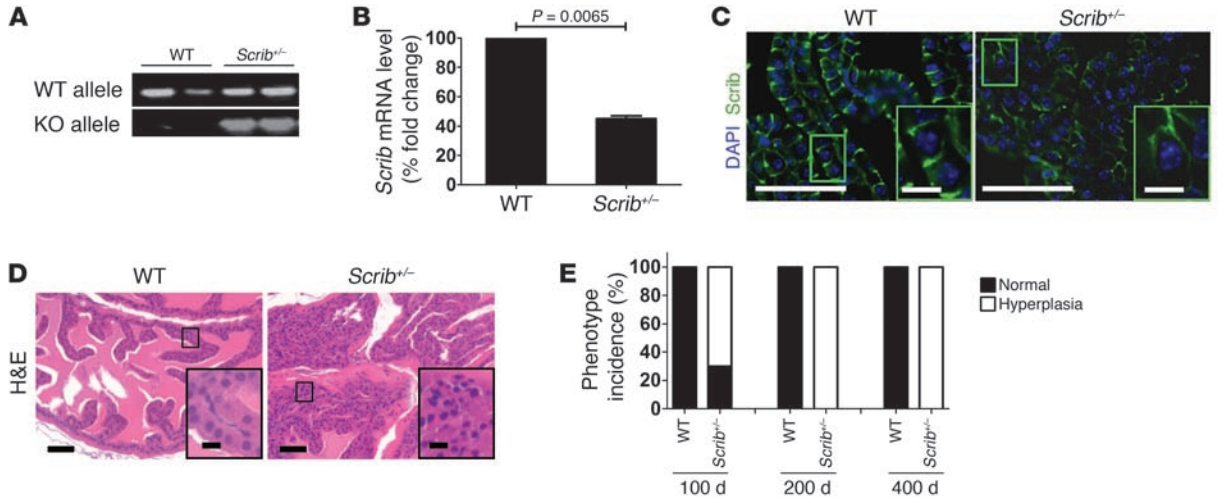

Figure 2

Scrib heterozygosity predisposes to prostate hyperplasia. (**A**) PCR analysis of genomic DNA to detect WT (290 bp) and KO (550 bp) *Scrib* alleles in *Scrib*$^{+/-}$ and WT prostate. (**B**) qRT-PCR for *Scrib* mRNA confirmed a significant, 55% reduction in *Scrib*$^{+/-}$ compared with WT prostates ($P = 0.0065$, unpaired *t* test). Error bars indicate SD. (**C**) Scrib IF staining of WT and *Scrib*$^{+/-}$ hyperplastic prostate. (**D**) Representative H&E images of normal WT and hyperplastic *Scrib*$^{+/-}$ prostate (400 days). (**E**) Phenotype incidence in WT and *Scrib*$^{+/-}$ mice at 100, 200, and 400 days ($n \geq 10$). Scale bars: 50 μm (larger panels) and 10 μm (insets).

ably, 7 of 10 *Scrib*$^{+/-}$ mice were predisposed to prostate hyperplasia (Figure 2), while histologically normal tissues included the intestine, liver, lung, stomach, pancreas, kidney, and bladder (data not shown). PCR analysis of genomic DNA confirmed recombination of the LoxP-flanked *Scrib* allele in *Scrib*$^{+/-}$ prostate tissue (Figure 2A) and quantitative RT-PCR (qRT-PCR) showed a significant, 55% reduction in *Scrib* mRNA isolated from *Scrib*$^{+/-}$ prostate tissue compared with WT prostate (Figure 2B). Immunofluorescence (IF) to detect Scrib revealed that WT epithelium displays uniform Scrib expression along the basolateral membrane that is prominent at tight junctions (Figure 2C). Although *Scrib*$^{+/-}$ lesions appeared to display a decrease in Scrib expression, statistical analysis of Scrib intensity revealed this was not significant (Figure 2C and Supplemental Figure 2A). Importantly, no difference in Scrib intensity was established between *Scrib*$^{+/-}$ hyperplastic and non-hyperplastic prostate epithelium, indicating that loss of heterozygosity (LOH) had not taken place (Supplemental Figure 2A), and to our knowledge, Scrib LOH has not been reported in the literature.

To determine whether *Scrib* heterozygosity is sufficient to drive neoplastic progression, male cohorts of WT and *Scrib*$^{+/-}$ littermates were generated and aged to 200 and 400 days ($n \geq 10$). Histological analysis revealed normal branched and single-layered prostate epithelium in WT mice at all time points (Figure 2, D and E). In contrast, all *Scrib*$^{+/-}$ mice displayed multifocal prostate hyperplasia (predominantly in the anterior lobe) at 200 and 400 days (100% incidence). *Scrib*$^{+/-}$ prostate lesions exhibited lumen overcrowding and a marked increase in mitotic figures (Figure 2D), indicating that *Scrib* heterozygosity predisposes to prostate hyperplasia. Further investigation of smaller cohorts revealed that multifocal prostate hyperplasia is present in *Scrib*$^{+/-}$ mice as early as 50 days (50% incidence), while WT mice displayed normal prostate epithelium ($n = 6$). Aging to 540 days did not cause neoplastic progression. Multifocal prostate hyperplasia was observed in *Scrib*$^{+/-}$ mice at 540 days, with 100% penetrance ($n = 8$). Indeed, an average of 17%–42% prostatic ducts displayed hyperplastic foci (50–540 days) that contained a similar packing density of cells, illustrating the general multifocal nature of this phenotype (Supplemental Figure 2, B and C). Noticeably, one 540-day-old *Scrib*$^{+/-}$ mouse developed a pancreatic preinvasive ductal lesion, and 4 of 8 (50%) were predisposed to lung adenocarcinomas (I. Elsum, unpublished observations). None of these lesions were observed in WT mice at 540 days ($n = 5$).

Characterization of Scrib$^{+/-}$ *prostate hyperplasia.* Assessment of the proliferation marker PCNA by IHC revealed a significant, 4.8-fold increase in the number of PCNA-positive cells in *Scrib*$^{+/-}$ prostate hyperplasia compared with WT prostate at 400 days (Figure 3A). However, no change in apoptosis was detected at this time point, as determined by active caspase-3 IHC (Supplemental Figure 2D). To ascertain which population of cells were proliferating, we analyzed basal (cytokeratin-5), and luminal (cytokeratin-8) lineage markers by IHC (Supplemental Figure 2E). *Scrib*$^{+/-}$ prostate hyperplastic cells stained positively for cytokeratin-8, whereas the distribution of cytokeratin-5–positive basal cells resembled that in WT prostate tissue. Together, these data indicate that *Scrib* heterozygosity is an initiating event in murine prostate hyperplastic growth and that Scrib deficiency induces proliferation, reflecting expansion of the luminal cell lineage.

To determine whether epithelial polarity is lost in *Scrib*$^{+/-}$ prostate lesions, we assessed the localization of markers for the apical (p-ERM) and lateral (E-cadherin) cell surfaces (Figure 3B). In WT prostate epithelial cells, E-cadherin was detected on the lateral surface and p-ERM was restricted to the apical surface. E-cadherin participates in adherens junctions, whereas p-ERM has been shown to play a role in mediating cell shape, adhesion, and motility (30). In contrast, *Scrib*$^{+/-}$ hyperplastic lesions displayed mislocalized E-cadherin, yet no significant difference in E-cadherin intensity was observed between WT and *Scrib*$^{+/-}$ prostate epithelium (Supplemental Figure 2F). The enrichment and misdistribution of p-ERM along the plasma membrane circumference suggest expansion and reorganization of the apical domain (30), consistent with a loss of apical-basal polarity (31). Loss of polarity within *Scrib*$^{+/-}$ hyperplastic lesions was further exemplified by IF

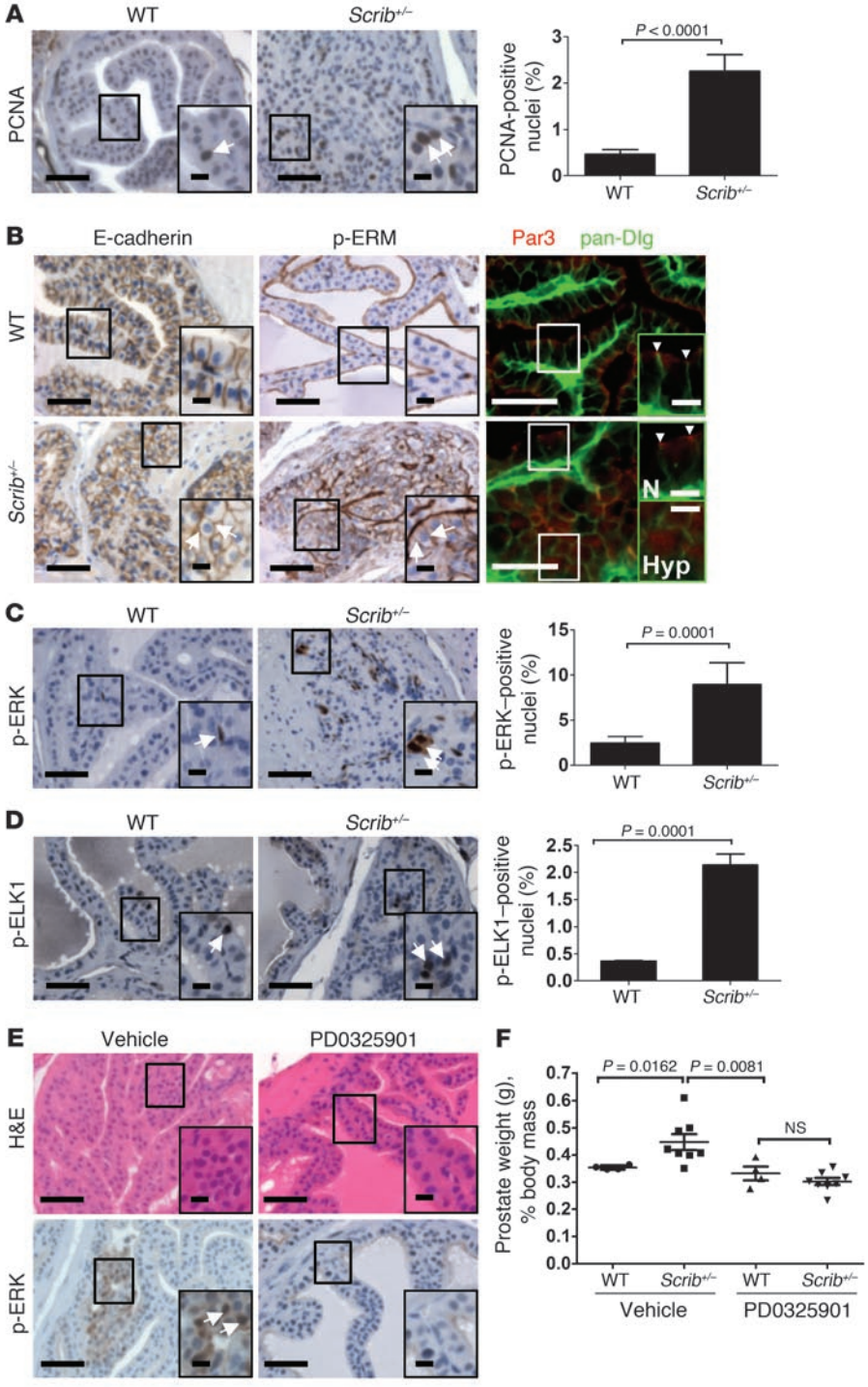

Figure 3
Elevated Ras/MAPK signaling is required for Scrib-deficient prostate hyperplasia. (**A**) PCNA IHC shows a significant increase in PCNA-positive cells in *Scrib*$^{+/-}$ lesions (2.26% ± 0.62%, mean ± SD) compared with WT (0.47% ± 0.09%, $P < 0.0001$, unpaired *t* test, 400 days). (**B**) IHC in *Scrib*$^{+/-}$ hyperplastic foci revealed aberrant E-cadherin and p-ERM compared with WT tissue. Arrows indicate aberrant expression. Right column: IF to detect Par3 (red) and pan-Dlg (green) shows that these polarity regulators are mislocalized in *Scrib*$^{+/-}$ prostate hyperplasia compared with WT prostate (400 days). N, normal *Scrib*$^{+/-}$ tissue; Hyp, hyperplastic *Scrib*$^{+/-}$ tissue. Arrowheads indicate Par3 accumulation at tight junctions. (**C**) IHC revealed a significant elevation in p-ERK–positive nuclei in *Scrib*$^{+/-}$ lesions compared with WT (unpaired *t* test, 400 days). (**D**) IHC revealed a significant elevation in p-ELK1–positive nuclei in *Scrib*$^{+/-}$ lesions compared with WT (unpaired *t* test, 400 days). (**E**) Representative H&E images of *Scrib*$^{+/-}$ prostates administered vehicle or PD0325901 (20 mg/kg, 5 days on, 2 days off for 3 weeks at 230–260 days of age), and p-ERK staining showing efficient MEK inhibition. (**F**) *Scrib*$^{+/-}$ prostate weight is significantly decreased upon MEK inhibition (0.30 ± 0.04 g, mean ± SD) compared with administration of vehicle (0.45 g ± 0.08, $P = 0.0003$, Mann-Whitney *U* non-parametric test), similar to the level in WT prostate ($P = 0.4606$, Mann-Whitney *U* non-parametric *t* test). Scale bar: 50 μm (larger panels) and 10 μm (insets). Error bars indicate SD.

staining for core apical (Par3) and basolateral (Dlg) components of the polarity program (Figure 3B). In WT prostate epithelium, Par3 localized apically, with prominent accumulation at tight junctions, while pan-Dlg localized to the basolateral membrane. *Scrib*$^{+/-}$ hyperplastic lesions displayed the mis-distribution of Par3 throughout the cytoplasm and Dlg along the circumference of the membrane. These data support previous work showing that loss of Scribble complex members is sufficient to mislocalize key polarity proteins and impair tissue and cellular polarity (6, 32–34).

Scrib$^{+/-}$ *prostate hyperplasia is dependent on Ras/MAPK signaling.* We and others have previously shown that SCRIB loss stimulates Ras/MAPK signaling in vitro, suggesting that SCRIB negatively regulates the Ras/MAPK cascade to suppress tumorigenesis (22, 23). We hypothesized that Scrib loss deregulates the Ras/MAPK pathway to facilitate prostate hyperplastic growth in mice. To test this hypothesis, we analyzed phosphorylation of the MAPK signaling molecule ERK. As determined by IHC, *Scrib*$^{+/-}$ prostate hyperplasia specifically displayed a significant, 3.7-fold increase in nuclear p-ERK expres-

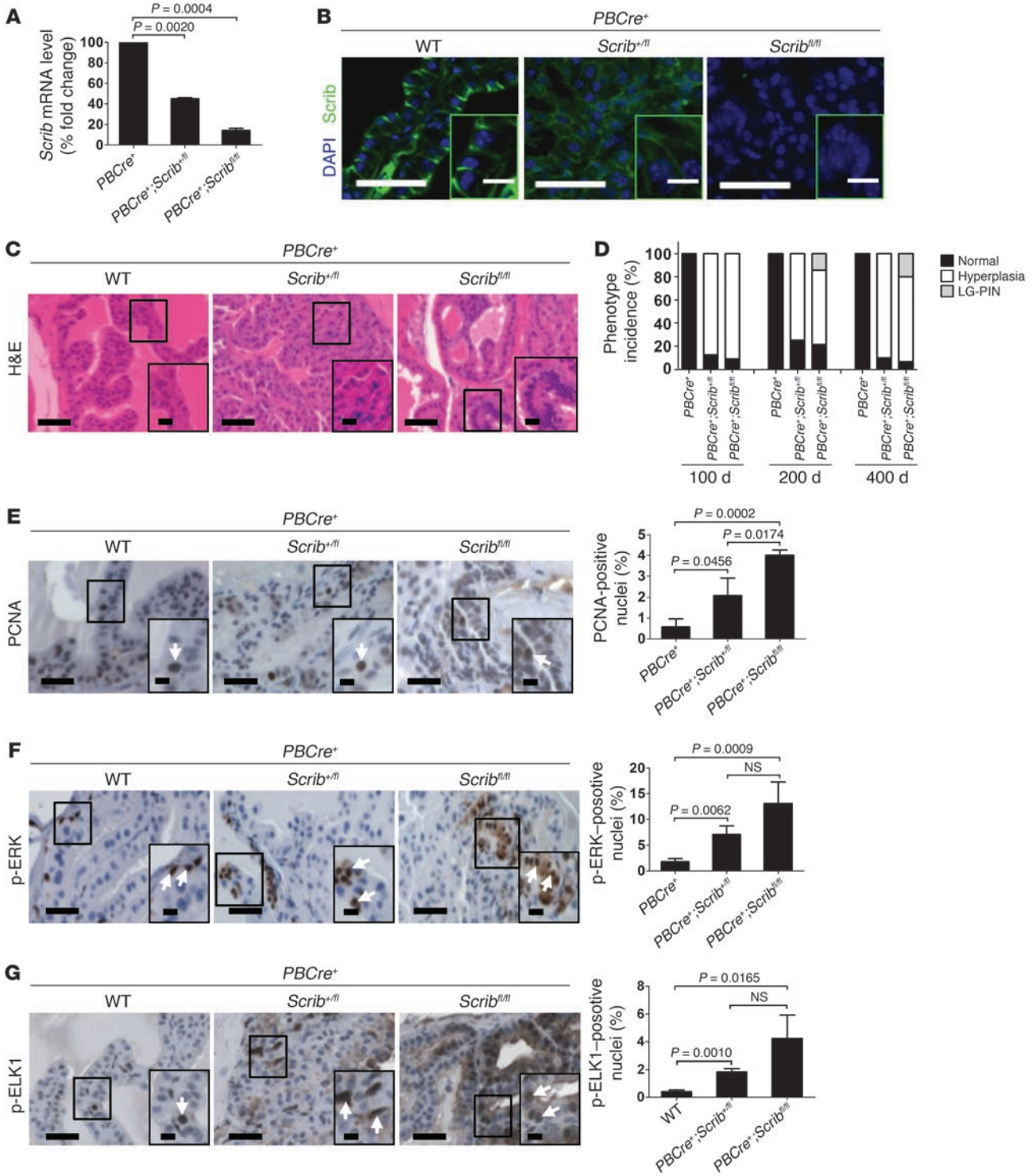

Figure 4

Biallelic *Scrib* loss causes prostate neoplasia. (**A**) *Scrib* mRNA is decreased in *PBCre*$^{+}$*;Scrib*$^{+/fl}$ (45.2%) and *PBCre*$^{+}$*;Scrib*$^{fl/fl}$ (14.5%) compared with *PBCre*$^{+}$ prostates at 400 days. (**B**) Scrib IF shows reduced Scrib expression in *PBCre*$^{+}$*;Scrib*$^{fl/fl}$ prostate epithelium (400 days). (**C**) Representative H&E images of *PBCre*$^{+}$, *PBCre*$^{+}$*;Scrib*$^{+/fl}$, and *PBCre*$^{+}$*;Scrib*$^{fl/fl}$ prostates (400 days). (**D**) Prostate phenotype incidence at 100, 200, and 400 days ($n \geq 10$). (**E**) PCNA IHC shows a significant increase in the number of PCNA-positive cells in *PBCre*$^{+}$*;Scrib*$^{fl/fl}$ mice (4.0% ± 0.24%) compared with *PBCre*$^{+}$*;Scrib*$^{+/fl}$ (2.1% ± 0.82%) and *PBCre*$^{+}$ mice (0.6% ± 0.38%) at 400 days. (**F**) p-ERK staining revealed a significant increase in MAPK signaling in *PBCre*$^{+}$*;Scrib*$^{+/fl}$ (7.1% ± 1.64%) and *PBCre*$^{+}$*;Scrib*$^{fl/fl}$ mice (13.1% ± 4.18%) compared with *PBCre*$^{+}$ controls (1.8% ± 0.58%) at 400 days. (**G**) p-ELK1 staining shows a significant increase in p-ELK1 expression in *PBCre*$^{+}$*;Scrib*$^{+/fl}$ (1.8% ± 0.25%) and *PBCre*$^{+}$*;Scrib*$^{fl/fl}$ (4.2% ± 1.67%) compared with WT tissue (0.4% ± 0.13%) at 400 days. Arrows indicate positive nuclei. Scale bars: 50 μm (larger panels) and 10 μm (insets). Data are mean ± SD; $n = 3$; *P* values represent unpaired *t* test. Error bars indicate SD.

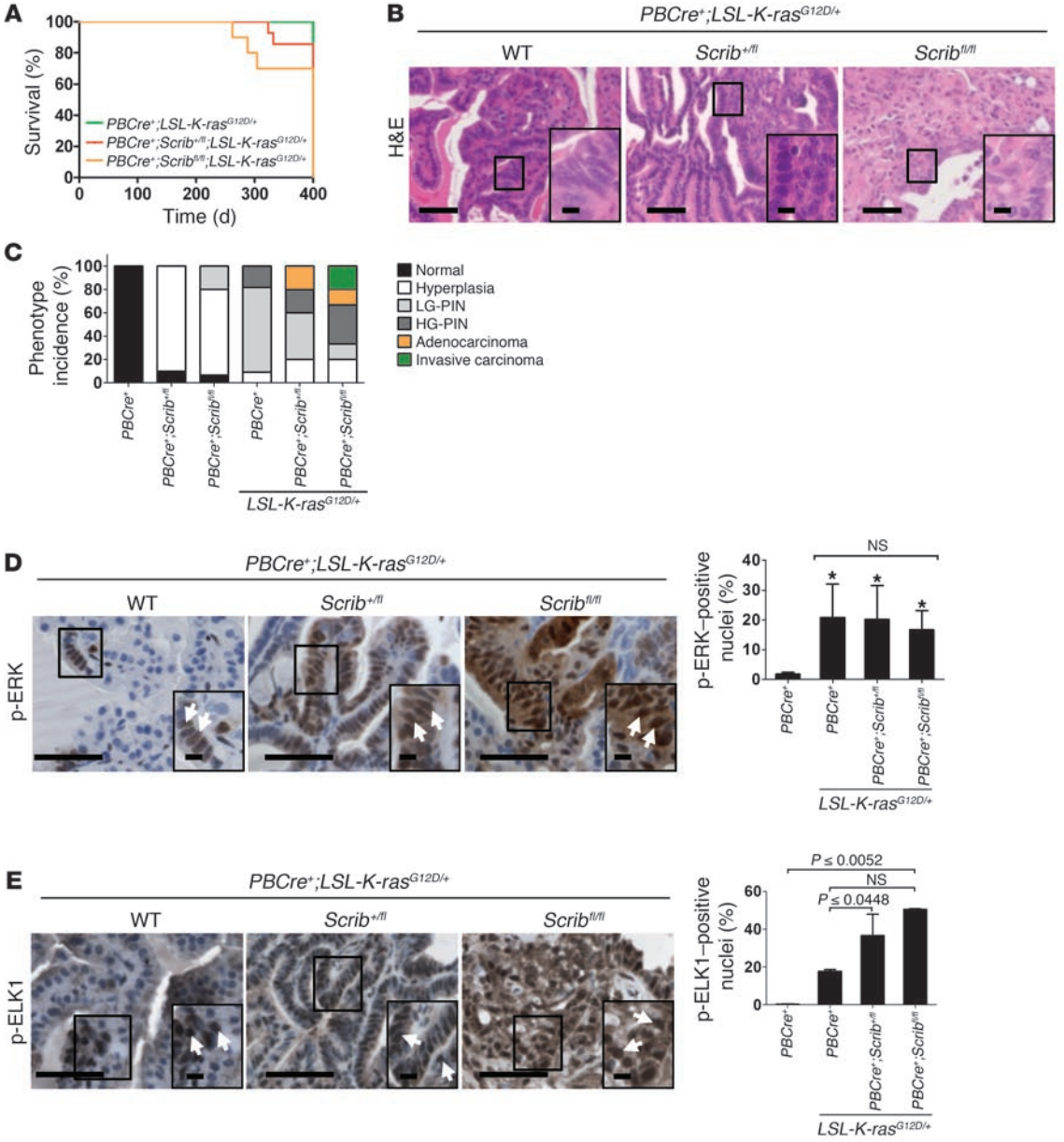

Figure 5

Scrib loss and K-ras hyperactivation cooperate to facilitate prostate tumor progression. (**A**) Kaplan-Meier survival plot shows a significant reduction in *PBCre*$^+$*;Scrib*$^{fl/fl}$*;LSL-K-ras*$^{G12D/+}$ average survival (372 days) compared with *PBCre*$^+$*;LSL-K-ras*$^{G12D/+}$ mice ($\chi^2 = 4.20$, $P = 0.0449$, log-rank test, $n \geq 10$). (**B**) Representative H&E images of *PBCre*$^+$*;LSL-K-ras*$^{G12D/+}$, *PBCre*$^+$*;Scrib*$^{+/fl}$*;LSL-K-ras*$^{G12D/+}$, and *PBCre*$^+$*;Scrib*$^{fl/fl}$*;LSL-K-ras*$^{G12D/+}$ prostates (400 days). (**C**) Prostate phenotype incidence (400 days, $n \geq 10$). (**D**) IHC to detect p-ERK reveals that the number of p-ERK–positive nuclei in *PBCre*$^+$*;LSL-K-ras*$^{G12D/+}$ (21% ± 11.24%), *PBCre*$^+$*;Scrib*$^{+/fl}$*;LSL-K-ras*$^{G12D/+}$ (20% ± 11.41%), and *PBCre*$^+$*;Scrib*$^{fl/fl}$*;LSL-K-ras*$^{G12D/+}$ (17% ± 6.35%) prostate tumors was significantly elevated compared with control prostate (*$P \leq 0.0496$), yet no statistical difference was determined between the double mutants and K-ras activation alone ($P > 0.6168$) at 400 days. (**E**) IHC to detect p-ELK1 revealed a significant increase in p-ELK1 expression in *PBCre*$^+$*;Scrib*$^{+/fl}$*;LSL-K-ras*$^{G12D/+}$ (36.6% ± 6.54%), and *PBCre*$^+$*;Scrib*$^{fl/fl}$*;LSL-K-ras*$^{G12D/+}$ (50.5% ± 0.43%) prostate lesions compared with *PBCre*$^+$*;LSL-K-ras*$^{G12D/+}$ (17.7% ± 0.55%, $P \leq 0.0448$) and *PBCre*$^+$ (0.4% ±0.07, $P \leq 0.0052$) prostate epithelium at 400 days. Scale bars: 50 μm (larger panels) and 10 μm (insets). In **D** and **E**, data are mean ± SD; n = 3; *P* values represent unpaired *t* test. Error bars indicate SD.

sion compared with WT epithelium, indicating that Scrib deficiency elevates Ras/MAPK signaling (Figure 3C and Supplemental Figure 2G). Accordingly, expression of p-ELK1, a downstream transcription factor target of p-ERK (35), was also significantly increased in *Scrib*$^{+/-}$ hyperplastic lesions compared with WT tissue (Figure 3D). Activation of the MAPK cascade was further confirmed by elevated cytoplasmic p-MEK expression in *Scrib*$^{+/-}$ hyperplastic foci (Supplemental Figure 2H). These data are consistent with the notion that Scrib plays a tumor-suppressive role within the murine prostate by regulating the Ras/MAPK pathway.

To directly test this hypothesis, we treated *Scrib*$^{+/-}$ mice with the commercially available MEK inhibitor PD0325901 (20 mg/kg,

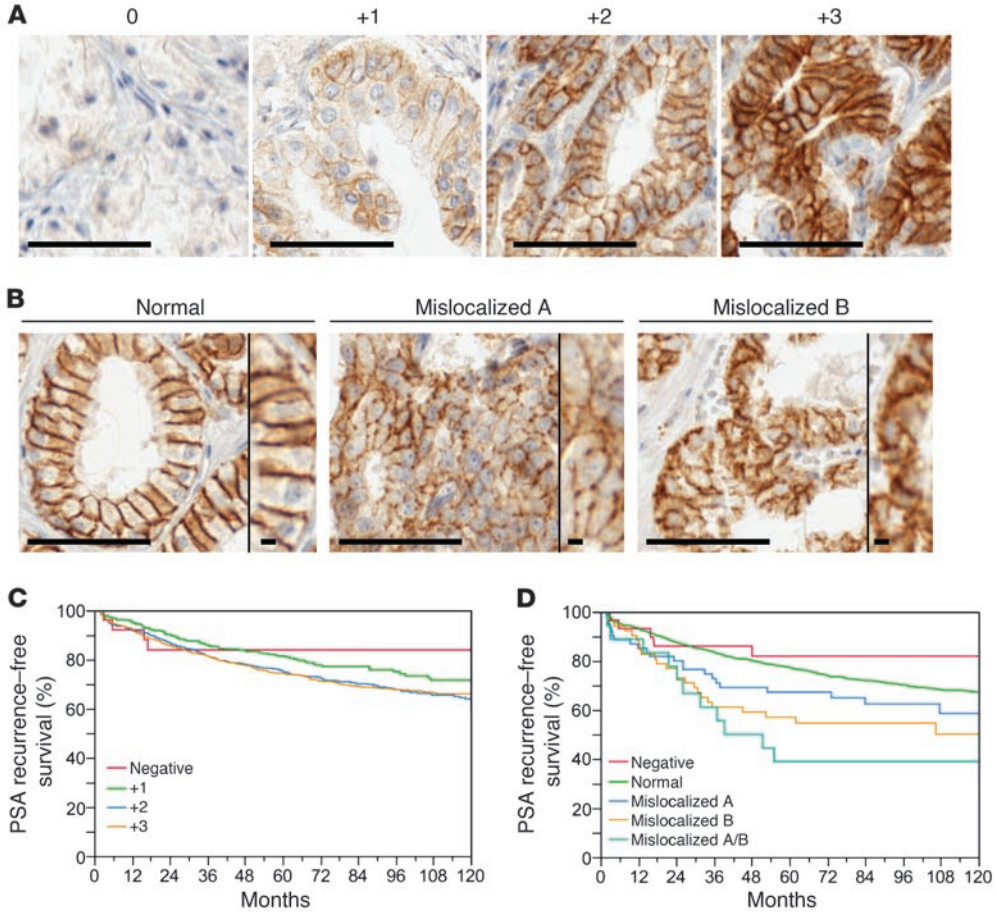

Figure 6

Human prostate tissue microarray. Representative images of TMA samples stained by IHC to detect SCRIB indicating the scoring strategy employed to grade SCRIB intensity (0 negative, +1 weak, +2 moderate, and +3 strong) (**A**) and mislocalization (**B**). Scale bars: 50 μm (larger panels) and 10 μm (insets). Samples displaying uniform basolateral membrane expression were designated as normal. Mislocalized expression was classified as clustered accumulation of SCRIB (group A: at cell-cell junctions; group B: along the membrane circumference; group A/B displays features of groups A and B). Scale bars: 50 μm (larger panels) and 10 μm (insets). (**C**) Kaplan-Meier plot indicates no significant difference between overall SCRIB intensity and PSA recurrence–free survival (P = 0.0687, log-rank test). Moreover, negative samples showed no significant difference in PSA recurrence–free survival compared with positive samples (P > 0.2196, log-rank test). (**D**) Kaplan-Meier plot comparing normal and mislocalized SCRIB expression revealed a significant reduction in PSA recurrence–free survival for all modes of mislocalization (P = 0.0001, log-rank test).

5 days on and 2 days off for 3 weeks) at 230–260 days of age (n = 8), when multifocal prostate hyperplasia is usually observed. Histological analysis revealed a marked decrease in hyperplastic foci in *Scrib*$^{+/-}$ mice administered PD0325901 compared with the vehicle (Figure 3E). Effective inhibition of p-ERK expression in response to the MEK inhibitor was confirmed by p-ERK IHC (Figure 3E and Supplemental Figure 3A). PD0325901 administration significantly reduced *Scrib*$^{+/-}$ prostate weight compared with the vehicle, and the level was similar to that in WT littermate controls (Figure 3F). *Scrib*$^{+/-}$ mice receiving PD0325901 also showed a significant, 2.4-fold reduction in PCNA expression compared with those receiving vehicle, indicating that MEK inhibition decreased proliferation in this setting (Supplemental Figure 3B). Notably, no phenotypic difference was detected by H&E analysis in WT littermates receiving the MEK inhibitor compared with the vehicle, consistent with the lack of a significant difference in prostate weight (P = 0.3429, Mann-Whitney U test, n = 4) (Figure 3F and Supplemental Figure 3C). IHC to detect p-ERK confirmed efficient MEK inhibition in WT epithelium (Supplemental Figure 3D).

Taken together, these data indicate that MEK inhibition is sufficient to rescue prostate hyperplasia in the context of Scrib deficiency and that intact Ras/MAPK signaling is required for prostate hyperplastic growth induced by Scrib depletion. Nevertheless, we cannot rule out the possibility that additional genetic/epigenetic changes may contribute to the Scrib-deficient phenotype in this setting.

Biallelic Scrib loss promotes neoplastic tumor progression. We next determined whether complete Scrib inactivation in the prostate could facilitate prostate cancer growth. Given that *Scrib*-KO mice are neonatal lethal, we employed *Cre*-LoxP technology to deplete Scrib expression specifically within the prostate epithelium. *Scrib* floxed mice were crossed to the *PBCre* transgenic line (36), and male cohorts of *PBCre*$^{+}$, *PBCre*$^{+}$;*Scrib*$^{+/fl}$, and *PBCre*$^{+}$;*Scrib*$^{fl/fl}$ mice were established and aged.

We confirmed *PBCre*-mediated recombination in the prostate by crossing *PBCre*$^{+}$ mice to the *Rosa26* reporter strain (37) and per-

forming LacZ staining (Supplemental Figure 4A). *Scrib* loss was verified by means of qRT-PCR (Figure 4A). *Scrib* mRNA was significantly reduced in *PBCre*$^+$;*Scrib*$^{+/fl}$ and *PBCre*$^+$;*Scrib*$^{fl/fl}$ prostates compared with those of *PBCre*$^+$ controls. Consistent with mRNA expression data, negligible levels of Scrib were detected by IF in *PBCre*$^+$;*Scrib*$^{fl/fl}$ prostate epithelium (Figure 4B).

Histological analysis revealed that *PBCre*$^+$;*Scrib*$^{+/fl}$ mice phenocopied *Scrib*$^{+/-}$ animals, displaying multifocal prostate hyperplasia at 100, 200, and 400 days (88%, 75%, and 90% incidence respectively; $n \geq 10$), indicating that the observed phenotype is intrinsic to the epithelial compartment (Figure 4, C and D). Analysis of *PBCre*$^+$;*Scrib*$^{fl/fl}$ prostate tissue revealed that biallelic *Scrib* loss facilitated neoplastic progression. At 200 and 400 days, *PBCre*$^+$;*Scrib*$^{fl/fl}$ mice displayed LG-PIN (14% and 20% incidence, respectively; $n \geq 10$) with solid and cribriform intraluminal proliferation of evidently atypical epithelial cells (Figure 4, C and D). Notably, PIN lesions were commonly associated with regions of hyperplasia.

IHC to detect the proliferation marker PCNA demonstrated that *PBCre*$^+$;*Scrib*$^{fl/fl}$ prostate lesions display a significant, 1.9- and 6.9-fold increase in PCNA expression compared with *PBCre*$^+$;*Scrib*$^{+/fl}$ and *PBCre*$^+$ mice, respectively (Figure 4E). In addition, *PBCre*$^+$;*Scrib*$^{fl/fl}$ lesions showed a small increase in the number of cells expressing the apoptotic marker active caspase-3; however, this elevation was not significantly different compared with WT and *PBCre*$^+$;*Scrib*$^{+/fl}$ mice (Supplemental Figure 4B).

Consistent with the *Scrib*$^{+/-}$ model, we observed activation of the Ras/MAPK cascade in prostate-specific Scrib–deficient lesions (Figure 4F). IHC for p-ERK showed a significant, 3.9- and 7.2-fold increase in the number of positive p-ERK nuclei in *PBCre*$^+$;*Scrib*$^{+/fl}$ and *PBCre*$^+$;*Scrib*$^{fl/fl}$ mice, respectively, compared with *PBCre*$^+$ controls. These data correlated with a significant increase in the downstream target of p-ERK, p-ELK1 (Figure 4G). These results further illustrate that Scrib loss facilitates prostate tumorigenesis through deregulated Ras/MAPK signaling in prostate epithelial cells.

K-ras activation and Scrib loss cooperate to facilitate prostate tumor progression. Loss of scrib and oncogenic ras cooperate to drive invasive cancer in *Drosophila* (24, 38). In addition, despite the low frequency of *RAS* mutations in human prostate cancer (39), RAS/RAF signaling is one of the three most common pathways to be altered in both primary and metastatic human prostate cancer tumors (39), and K-RAS deregulation and elevated MAPK signaling are common features (39, 40). To investigate the potential cooperation between Scrib deficiency and oncogenic Ras/MAPK signaling in prostate tumorigenesis, we generated and aged cohorts of male mice in which Scrib loss and hyperactivated K-ras (*LSL-K-ras*^{G12D}) were specifically induced in the prostate ($n \geq 10$). Several *PBCre*$^+$;*Scrib*$^{fl/fl}$;*LSL-K-ras*$^{G12D/+}$ mice (3 of 10) displayed signs of illness and were sacrificed prior to the 400 days end point (Figure 5A). Compared with the *PBCre*$^+$;*LSL-K-ras*$^{G12D/+}$ cohort, which survived to 400 days, *PBCre*$^+$;*Scrib*$^{fl/fl}$;*LSL-K-ras*$^{G12D/+}$ mice displayed a small yet significant reduction in average survival (372 days), suggesting that Scrib depletion and K-ras activation may cooperate to accelerate disease progression. Although 2 mice in the *PBCre*$^+$;*Scrib*$^{+/fl}$;*LSL-K-ras*$^{G12D/+}$ cohort became ill and were sacrificed before 400 days, no statistical difference in average survival was determined compared with single mutant or control cohorts.

PCR analysis of DNA isolated from the prostate revealed that recombination of the LoxP-flanked *LSL-K-ras*^{G12D} and *Scrib* alleles occurred in single and double transgenics, respectively, and not in *PBCre*$^+$ and *Cre*-negative controls (Supplemental Figure 4C). qRT-PCR analysis confirmed a reduction in *Scrib* mRNA in *PBCre*$^+$;*Scrib*$^{+/fl}$;*LSL-K-ras*$^{G12D/+}$ and *PBCre*$^+$;*Scrib*$^{fl/fl}$;*LSL-K-ras*$^{G12D/+}$ mice compared with controls (Supplemental Figure 4D).

Histological analysis of *PBCre*$^+$;*Scrib*$^{+/fl}$;*LSL-K-ras*$^{G12D/+}$ and *PBCre*$^+$;*Scrib*$^{fl/fl}$;*LSL-K-ras*$^{G12D/+}$ mice established that compound mutants were susceptible to accelerated tumor progression compared with mice with Scrib loss or K-ras activation alone (Figure 5, B and C). *PBCre*$^+$;*LSL-K-ras*$^{G12D/+}$ prostate glands displayed hyperplasia, LG-PIN, and high-grade PIN (HG-PIN) lesions (9%, 73%, and 18% incidence, respectively), consistent with a similar model (41). *PBCre*$^+$;*Scrib*$^{+/fl}$;*LSL-K-ras*$^{G12D/+}$ and *PBCre*$^+$;*Scrib*$^{fl/fl}$;*LSL-K-ras*$^{G12D/+}$ mice displayed HG-PIN (20% and 33% incidence respectively) and well-differentiated adenocarcinoma (20% and 13% incidence, respectively), and 3 of 15 (20%) *PBCre*$^+$;*Scrib*$^{fl/fl}$;*LSL-K-ras*$^{G12D/+}$ mice developed poorly differentiated invasive carcinoma (Figure 5, B and C). HG-PIN lesions displayed solid and occasional cribriform patterns with nuclear enlargement/elongation. Well-differentiated adenocarcinomas displayed well-maintained glandular differentiation, while poorly differentiated carcinoma showed more solid nests of tumor cells. All the aforementioned lesions displayed nuclear atypia, mitotic figures, and extensive overcrowding of the lumen as multicellular disorganized layers formed. In addition, all K-ras–induced prostate tumors (*PBCre*$^+$;*LSL-K-ras*$^{G12D/+}$, *PBCre*$^+$;*Scrib*$^{+/fl}$;*LSL-K-ras*$^{G12D/+}$, and *PBCre*$^+$;*Scrib*$^{fl/fl}$;*LSL-K-ras*$^{G12D/+}$) were associated with focal intestinal metaplasia, mirroring previous work (42).

To address the molecular mechanism underlying the cooperation between Scrib deficiency and K-ras activation to promote prostate cancer progression, we performed PCNA IHC (Supplemental Figure 4E). Compared with *PBCre*$^+$ controls, *PBCre*$^+$;*LSL-K-ras*$^{G12D/+}$, *PBCre*$^+$;*Scrib*$^{+/fl}$;*LSL-K-ras*$^{G12D/+}$, and *PBCre*$^+$;*Scrib*$^{fl/fl}$;*LSL-K-ras*$^{G12D/+}$ mutants all showed a significant increase in PCNA-positive cells, although Scrib loss did not result in a significant increase compared with K-ras activation alone. In addition, a significant elevation in the expression of the apoptosis marker active caspase-3 in *PBCre*$^+$;*LSL-K-ras*$^{G12D/+}$, *PBCre*$^+$;*Scrib*$^{+/fl}$;*LSL-K-ras*$^{G12D/+}$, and *PBCre*$^+$;*Scrib*$^{fl/fl}$;*LSL-K-ras*$^{G12D/+}$ prostate tumors compared with control mice was determined by means of IHC; however, no statistical difference was observed between double mutants and K-ras activation alone (Supplemental Figure 4F). IHC confirmed that all mutants displayed aberrant E-cadherin and p-ERM expression, indicating that polarity was lost (Supplemental Figure 4G). Taken together, these data indicate that aberrant proliferation, apoptosis, and loss of polarity in double mutants do not trigger accelerated tumor progression.

To confirm activation of Ras/MAPK signaling in K-ras mutants and to further understand the mechanism whereby Scrib loss and K-ras activation cooperate to accelerate prostate cancer progression, we analyzed the activity of the Ras/MAPK pathway. IHC to detect p-ERK confirmed activation of the Ras/MAPK cascade in all mutants expressing oncogenic K-ras (Figure 5D). Compared with *PBCre*$^+$ controls, the *PBCre*$^+$;*LSL-K-ras*$^{G12D/+}$, *PBCre*$^+$;*Scrib*$^{+/fl}$;*LSL-K-ras*$^{G12D/+}$, and *PBCre*$^+$;*Scrib*$^{fl/fl}$;*LSL-K-ras*$^{G12D/+}$ mutants showed a significant increase in p-ERK expression, yet IHC analysis was not sensitive enough to detect a significant increase in p-ERK expression in double mutants compared with *PBCre*$^+$;*LSL-K-ras*$^{G12D/+}$ mice. Nonetheless, IHC to detect the p-ERK downstream target p-ELK1 revealed a significant increase in *PBCre*$^+$;*Scrib*$^{+/fl}$;*LSL-K-ras*$^{G12D/+}$ (2.1-fold) and *PBCre*$^+$;*Scrib*$^{fl/fl}$;*LSL-K-ras*$^{G12D/+}$ (2.9-fold) mutants compared with *PBCre*$^+$;*LSL-K-ras*$^{G12D/+}$ mice (Figure 5E). These data indicate that Scrib loss and oncogenic K-ras cooperate to promote prostate cancer progression via ELK1 activation, which leads to

transcriptional activation of a variety of growth-regulatory genes that include the *c-fos* proto-oncogene (35). Although p-ELK1 is a direct target of the Ras/MAPK cascade, it is possible that additional pathways that mediate ELK1 activation, including JNK and p38 signaling (43), may also underpin the synergistic relationship between Scrib loss and K-ras activation in this setting.

SCRIB mislocalization predicts poor survival in human prostate cancer. To determine whether SCRIB is deregulated in human prostate cancer, we performed IHC to detect SCRIB on a prostate tissue microarray consisting of more than 2,000 hormone-naive patients with full clinical follow-up data (Supplemental Table 1) and assessed the intensity and mislocalization of SCRIB (Figure 6, A and B, Supplemental Tables 2 and 3, and ref. 44). SCRIB expression was observed in 98% (2,086 of 2,122) of all assessable samples. Non-assessable samples were omitted from our analysis (where clinical data were missing or tissue/tumor sections were absent; n = 1,139). SCRIB intensity significantly correlated with tumor stage, Gleason grade, and prostate-specific antigen (PSA) level (Supplemental Table 2). Despite a small, yet significant difference between low (+1) and moderate (+2) SCRIB expression predicting for poor survival (P = 0.0369, log-rank test), there was no association between moderate (+2) and high (+3) SCRIB expression (Figure 6C). Moreover, negative samples did not statistically correlate with PSA recurrence–free survival compared with positive samples and were predominantly atrophic (n = 31).

SCRIB mislocalization was observed in 7.1% (151 of 2,122) of all samples and positively correlated with tumor stage, Gleason grade, and PSA level (Supplemental Table 3). Mislocalization was categorized into 3 subgroups: punctate cell-cell junction clustering (A), accumulation along the circumference of the membrane (B), and a combination of features of both categories (A/B) (Figure 6B). Importantly, all modes of mislocalization significantly predicted for poor PSA recurrence–free survival (Figure 6D and Supplemental Table 3). This association may be attributable to the fact that SCRIB mislocalization has been linked to loss of function (17, 26, 45). Taken together, this evidence suggests that mislocalization of the polarity regulator SCRIB correlates with poor survival in human prostate cancer, highlighting the need for further investigation of polarity regulators in prostate cancer.

Discussion

We have described what we believe to be a novel model of prostate cancer and have demonstrated that while Scrib depletion alone is a poor initiator of prostate neoplasia, following an oncogenic event, loss of Scrib contributes to tumor progression. These data establish a unique link between prostate cancer and loss of an epithelial polarity regulator and demonstrate that loss of cellular polarity is a tumor-initiating event and not simply a consequence of cellular transformation. Mechanistically, we have established that Ras/MAPK signaling is required for Scrib-deficient prostate hyperplasia in vivo using a MEK inhibitor, validating previous in vitro work (22, 23). Recent studies in human keratinocytes suggest that the mechanism whereby SCRIB suppresses RAS/MAPK signaling could result from a direct interaction between SCRIB and ERK, which diminishes ERK activation (22). The emerging complexity of SCRIB-mediated regulation of the RAS/MAPK cascade is further illustrated by SCRIB interactions with RSK2, a negative regulator of the pathway (46), and GIT1, an ARF-GAP that can act as a MEK-ERK scaffold (47, 48).

Furthermore, we demonstrate that Scrib loss and oncogenic K-ras cooperate to accelerate disease progression in mice, illustrating the multistep nature of prostate cancer progression and providing evidence to support published *Drosophila* in vivo and mammalian in vitro studies (23, 24). Mechanistically, this synergism correlated with elevated p-ELK1 expression, presenting a direct mechanism whereby Scrib loss and oncogenic K-ras synergize to drive prostate cancer progression. While elevated p-ELK1 expression is likely to reflect enhanced Ras/MAPK signaling (35), future work will be necessary to determine whether additional Scrib-mediated pathways, such as JNK, p38, Wnt, and Notch signaling, may also play a role in the cooperative relationship between Scrib loss and K-ras activation to drive murine prostate tumor progression (5). Notably, JNK and p38 signaling have previously been reported to activate ELK1 to mediate transcription of growth regulatory genes (43), and oncogenic Wnt signaling has been shown to cooperate with K-ras activation to accelerate prostate cancer progression in mice (41).

Currently, evidence for the role of SCRIB in human prostate cancer is conflicting. Although SCRIB maps to 8q24, which also harbors c-Myc and prostate stem cell antigen (PSCA) and is frequently amplified in prostate cancer (49), a microarray dataset shows a decrease in *Scrib* mRNA in human prostate carcinoma (50). Furthermore, integrated genomic profiling has recently shown that 33% (77 of 230, all samples, z-score threshold ± 1.0) of human prostate cancers display deregulated SCRIB expression (39). We have gained key insights into human prostate cancer, where mislocalization rather than loss of SCRIB predicts for poor survival. Given this result, it is tempting to speculate that SCRIB mislocalization reflects aberrant SCRIB function, as suggested by previous studies (17, 25, 26). Functional analysis of LRR SCRIB point mutant proteins shows restriction of SCRIB to the cytoplasm that is associated with loss of function in *Caenorhabditis elegans* (25), *Drosophila* (26), mice (29), and a human breast cancer cell line (17). The latter study postulates that the mislocalization of SCRIB disrupts its ability to recruit the β-PIX/GIT1 complex, resulting in Rac activation and tumor growth (17). Consequently, the mislocalization we observe in human prostate cancer is likely to inhibit its tumor-suppressive function. Despite advancements in large-scale sequencing, mutations in SCRIB that could cause its mislocalization remain to be identified in human cancers, suggesting other events may underlie this process.

Consistent with our findings in human prostate cancer, SCRIB is deregulated/mislocalized in human colorectal, breast, and endometrial cancers (14–18). This evidence supports the notion that SCRIB may play a broader role in epithelial tissue homeostasis, and our conditional Scrib-KO mouse model presents a potentially invaluable tool to address this prospect further.

Importantly, we show that *Scrib*$^{+/-}$ prostate hyperplasia displayed mis-distribution of several polarity regulators and adhesion proteins, correlating with previous work (16, 32, 34) and raising the possibility that human prostate tumors displaying SCRIB mislocalization could exhibit a general polarity defect. However, it is possible that our study underestimates the number of tumors that have lost polarity, as this event may also stem from additional polarity regulator defects not associated with SCRIB deregulation. Our future work will assess the distribution of core polarity proteins in human prostate cancer and the molecular mechanism for codependent localization of polarity regulators to further understand the link between aberrant cellular polarity and prostate cancer.

Taken together, our data indicate that Scrib deficiency is a poor initiator of cancer and that an additional oncogenic or tumor suppressor mutation is required for Scrib deregulation to con-

tribute to tumor progression. Mechanistic insights into how loss of polarity occurs in prostate epithelium and its impact on tumor onset and progression will improve our understanding of prostate cancer etiology and may facilitate the discovery of innovative prognostic factors and chemotherapeutic avenues involving the polarity network.

Methods

Derivation of Scrib-deficient mice. To inactivate Scrib, we constructed a *Scrib* targeting vector harboring a 5′ LoxP site in intron 3 and a 3′ LoxP site and Frt-flanked PGK-neomycin selection cassette within intron 13 (Supplemental Figure 1A). Excision of the Neo cassette was achieved by crossing $Scrib^{fl\text{-}Neo}$ mice to *Actin-FLPe* mice, producing the conditional *Scrib* floxed allele ($Scrib^{fl}$). To generate the *Scrib*-KO allele, we crossed $Scrib^{+/fl}$ mice to the germline *Cre*-deleter strain (27) and analyzed littermates. Founder mice were validated by Southern blot analysis of genomic DNA from ES cell clones (see Supplemental Figure 1B).

Experimental animals. To generate $PBCre^{+};Scrib^{fl}$ mice, we crossed female $Scrib^{+/fl}$ FVB/n mice with male *ARR2PBi-Cre* (*PBCre*) FVB/n transgenic mice (36), a gift from Christopher Hovens (Australian Prostate Cancer Research Centre, Epworth Hospital, Melbourne, Victoria, Australia). Male $PBCre^{+};Scrib^{+/fl}$ offspring were crossed to female $Scrib^{+/fl}$ mice to generate $PBCre^{+};Scrib^{fl/fl}$ mice. Females harboring an $LSL\text{-}K\text{-}ras^{G12D}$ allele (51) on a B6.129 background were backcrossed at least 6 times to FVB/n mice and crossed to male $PBCre^{+};Scrib^{+/fl}$ FVB/n mice. Male $PBCre^{+};Scrib^{+/fl};LSL\text{-}K\text{-}ras^{G12D/+}$ offspring were then bred to female $Scrib^{+/fl}$ mice to generate $PBCre^{+};Scrib^{fl/fl};LSL\text{-}K\text{-}ras^{G12D/+}$ mice.

Genotyping. Mice were genotyped from genomic DNA isolated from toe biopsies. WT and LoxP-flanked *Scrib* alleles were detected using the primers ScribF, 5′-GCCATGGTGGCAGAGGTTGG-3′ and ScribR1, 5′-TGCTTTCTCCCAGACTCAGG-3′ (WT, 290 bp; $Scrib^{fl}$, 390 bp). The recombined *Scrib* allele was detected using ScribF2, 5′-GAGAAAGTTGGGCCTCAGTG-3′ and ScribR1 (550 bp). The PCR program employed was 95°C for 2 minutes, followed by 35 cycles of 94°C for 30 seconds, 56°C for 30 seconds, 72°C for 30 seconds, and an elongation step of 72°C for 10 minutes.

Histological analysis. Formalin-fixed, paraffin-embedded (FFPE) tissue sections were stained with H&E, and pathology was determined from multiple step-sections (n = 3–7 per animal) as described previously (52).

PD0325901 administration. PD0325901 was obtained from JS Research Chemicals Trading and delivered via oral gavage at 20 mg/kg. PD0325901 (8 mg/ml, dissolved in 0.5% hydroxypropyl-methylcellulose; 0.2% Tween 80) was delivered for 5 days on and 2 days off for 3 weeks, as previously optimized for murine prostate (53). Littermates were weighed daily for signs of distress; however, no appreciable toxicity was observed (i.e., >10% weight loss). Prostate wet weights were determined at harvest.

IHC and IF. IHC (FFPE samples) and IF (4% PFA-fixed cryosections) were carried out as described previously (54), except antigen retrieval was performed using Tris-EDTA (pH 9) (S237584, Dako) for p-ERM, E-cadherin, and PCNA staining. Primary antibodies included pan-Dlg 1:100 (05-427, Upstate), E-cadherin 1:400 (610181, BD Biosciences — Pharmingen), p-ezrin (Thr567)/radixin (Thr564)/moesin (Thr558) 1:200 (3141, Cell Signaling Technology), p-ELK1 (Ser383) 1:100 (ab32799, Abcam), p-ERK1/2 (Thr 202/Tyr204) 1:150 (4376, Cell Signaling Technology), PAR3 1:100 (NP_062565, Millipore), PCNA 1:200 (610665, BD Biosciences — Pharmingen), and Scrib 1:150 (SC1409, Santa Cruz Biotechnology Inc.). Negative control slides were run without primary antibody, and positive control slides were incorporated. IHC scoring was performed using MetaMorph 6.3 software (Molecular Devices) from 20 images per mouse (×40 magnification, BX-51 Olympus microscope). A minimum of 1,000 cells/mouse were counted. All analysis was carried out on anterior prostate lobes.

Western blot analysis. Western blotting was carried out using embryonic brain homogenates, as previously described (55).

qRT-PCR analysis. Prostate RNA was isolated using TRizol (Invitrogen), TURBO DNase treated (Ambion), and reverse transcribed with Superscript III (Invitrogen). Amplification of cDNA was performed by the StepOnePlus Real-Time PCR System (Applied Biosystems). Samples were normalized to *Gapdh*, and fold change was calculated by the $2^{-\Delta\Delta Ct}$ method (56). *Scrib* mRNA was detected using mqS-F, 5′-TGTCAGTGTCATCCAGTTCG-3′ and mqS-R, 5′-CTTCAATGCCCCTCTTCATC-3′.

Tissue microarray analysis. Hormone-naive radical prostatectomy specimens from 3,261 patients were obtained from the University Medical Center Hamburg-Eppendorf between 1992 and 2005 (Supplemental Table 1) (44). Follow-up data were available for 2,891 patients, ranging from 0.03 to 219 months (mean, 72.1 months). Tumor recurrence (biochemical recurrence) was defined as postoperative levels of total PSA of 0.1 ng/ml or greater and rising after initial undetectable total PSA. TMA FFPE sections were stained using a previously described IHC method (44). See Supplemental Table 4 for raw data.

Tissue microarray construction. One tissue core was punched from a representative tumor area and transferred in a TMA format as described previously (57). Based on 34βE12 IHC data from a previous study (58), 892 (27.4%) samples were excluded, as the basal cell marker indicated a lack of tumor cells in these cores.

Statistics. Statistical analysis was performed using GraphPad Prism 5 software. IHC scoring was analyzed statistically for each genotype (n = 3) using a 2-tailed unpaired t test, where a P value less than 0.05 was considered statistically significant. qRT-PCR reactions were performed in triplicate, and significance was calculated using a 2-tailed unpaired t test of the average fold change. The prostate weight for each genotype (n = 4–8) was statistically analyzed using the nonparametric Mann Whitney U test. The relationship between human SCRIB intensity/localization and clinical parameters was analyzed using the χ^2 likelihood test. Kaplan-Meier survival curves were compared with the log-rank test.

Study approval. All animal studies were approved by the Peter MacCallum Cancer Centre Animal Experimental Ethics Committee. The use of human tissue and clinical data was according to the Hamburger Krankenhaus Gesetz (§12 HmbKHG) and approved by the local Ethical Committee (University Medical Centre Hamburg-Eppendorf, Hamburg, Germany).

Acknowledgments

Many thanks go to Michael Durrant, Josh Noske, Olivia Cakebread, Samantha Williams, Ryan Galea, and Lorey Smith at the Peter MacCallum Cancer Centre for their technical assistance. D.A. Tuveson acknowledges the support of the University of Cambridge, Cancer Research UK, and Hutchison Whampoa Limited. P.A. Perez-Mancera received financial support from the Ministerio de Educación y Ciencia of Spain and from Fundación Caja Madrid. This work was supported by the Prostate Cancer Foundation of Australia (PCFA) and the National Health and Medical Research Council (NHMRC). P.O. Humbert is supported by an NHMRC career development fellowship.

Received for publication April 14, 2011, and accepted in revised form August 16, 2011.

Address correspondence to: Patrick O. Humbert, Cell Cycle and Cancer Genetics Laboratory, Peter MacCallum Cancer Centre, East Melbourne, VIC 3002, Australia. Phone: 61.0.3.96563526; Fax: 61.0.3.96561411; E-mail: Patrick.Humbert@petermac.org.

1. Nelson WJ. Adaptation of core mechanisms to generate cell polarity. *Nature*. 2003;422(6933):766–774.
2. Dow LE, Humbert PO. Polarity regulators and the control of epithelial architecture, cell migration, and tumorigenesis. *Int Rev Cytol*. 2007;262:253–302.
3. Wodarz A, Nathke I. Cell polarity in development and cancer. *Nat Cell Biol*. 2007;9(9):1016–1024.
4. Huang L, Muthuswamy SK. Polarity protein alterations in carcinoma: a focus on emerging roles for polarity regulators. *Curr Opin Genet Dev*. 2010; 20(1):41–50.
5. Humbert PO, Grzeschik NA, Brumby AM, Galea R, Elsum I, Richardson HE. Control of tumourigenesis by the Scribble/Dlg/Lgl polarity module. *Oncogene*. 2008;27(55):6888–6907.
6. Bilder D, Li M, Perrimon N. Cooperative regulation of cell polarity and growth by Drosophila tumor suppressors. *Science*. 2000;289(5476):113–116.
7. Nakagawa S, Huibregtse JM. Human scribble (Vartul) is targeted for ubiquitin-mediated degradation by the high-risk papillomavirus E6 proteins and the E6AP ubiquitin-protein ligase. *Mol Cell Biol*. 2000; 20(21):8244–8253.
8. Gardiol D, Kuhne C, Glaunsinger B, Lee SS, Javier R, Banks L. Oncogenic human papillomavirus E6 proteins target the discs large tumour suppressor for proteasome-mediated degradation. *Oncogene*. 1999; 18(40):5487–5496.
9. Nakagawa S, et al. Analysis of the expression and localisation of a LAP protein, human scribble, in the normal and neoplastic epithelium of uterine cervix. *Br J Cancer*. 2004;90(1):194–199.
10. Cavatorta AL, et al. Differential expression of the human homologue of drosophila discs large oncosuppressor in histologic samples from human papillomavirus-associated lesions as a marker for progression to malignancy. *Int J Cancer*. 2004;111(3):373–380.
11. Lisovsky M, et al. Cell polarity protein Lgl2 is lost or aberrantly localized in gastric dysplasia and adenocarcinoma: an immunohistochemical study. *Mod Pathol*. 2009;22(7):977–984.
12. Lisovsky M, Ogawa F, Dresser K, Woda B, Lauwers GY. Loss of cell polarity protein Lgl2 in foveolar-type gastric dysplasia: correlation with expression of the apical marker aPKC-zeta. *Virchows Arch*. 2010; 457(6):635–642.
13. Fuja TJ, Lin F, Osann KE, Bryant PJ. Somatic mutations and altered expression of the candidate tumor suppressors CSNK1 epsilon, DLG1, and EDD/hHYD in mammary ductal carcinoma. *Cancer Res*. 2004;64(3):942–951.
14. Gardiol D, Zacchi A, Petrera F, Stanta G, Banks L. Human discs large and scrib are localized at the same regions in colon mucosa and changes in their expression patterns are correlated with loss of tissue architecture during malignant progression. *Int J Cancer*. 2006; 119(6):1285–1290.
15. Kamei Y, et al. Human scribble accumulates in colorectal neoplasia in association with an altered distribution of beta-catenin. *Hum Pathol*. 2007; 38(8):1273–1281.
16. Navarro C, et al. Junctional recruitment of mammalian Scribble relies on E-cadherin engagement. *Oncogene*. 2005;24(27):4330–4339.
17. Zhan L, et al. Deregulation of scribble promotes mammary tumorigenesis and reveals a role for cell polarity in carcinoma. *Cell*. 2008;135(5):865–878.
18. Ouyang Z, Zhan W, Dan L. hScrib, a human homolog of Drosophila neoplastic tumor suppressor, is involved in the progress of endometrial cancer. *Oncol Res*. 2010;18(11–12):593–599.
19. Kallay LM, McNickle A, Brennwald PJ, Hubbard AL, Braiterman LT. Scribble associates with two polarity proteins, Lgl2 and Vangl2, via distinct molecular domains. *J Cell Biochem*. 2006;99(2):647–664.
20. Metais JY, Navarro C, Santoni MJ, Audebert S, Borg JP. hScrib interacts with ZO-2 at the cell-cell junctions of epithelial cells. *FEBS Lett*. 2005;579(17):3725–3730.
21. Takizawa S, et al. Human scribble, a novel tumor suppressor identified as a target of high-risk HPV E6 for ubiquitin-mediated degradation, interacts with adenomatous polyposis coli. *Genes Cells*. 2006; 11(4):453–464.
22. Nagasaka K, et al. The cell polarity regulator hScrib controls ERK activation through a KIM site-dependent interaction. *Oncogene*. 2010;29(38):5311–5321.
23. Dow LE, Elsum IA, King CL, Kinross KM, Richardson HE, Humbert PO. Loss of human Scribble cooperates with H-Ras to promote cell invasion through deregulation of MAPK signalling. *Oncogene*. 2008; 27(46):5988–6001.
24. Brumby AM, Richardson HE. scribble mutants cooperate with oncogenic Ras or Notch to cause neoplastic overgrowth in Drosophila. *EMBO J*. 2003; 22(21):5769–5779.
25. Legouis R, Jaulin-Bastard F, Schott S, Navarro C, Borg JP, Labouesse M. Basolateral targeting by leucine-rich repeat domains in epithelial cells. *EMBO Rep*. 2003;4(11):1096–1102.
26. Zeitler J, Hsu CP, Dionne H, Bilder D. Domains controlling cell polarity and proliferation in the Drosophila tumor suppressor Scribble. *J Cell Biol*. 2004; 167(6):1137–1146.
27. Lakso M, et al. Efficient in vivo manipulation of mouse genomic sequences at the zygote stage. *Proc Natl Acad Sci U S A*. 1996;93(12):5860–5865.
28. Murdoch JN, et al. Disruption of scribble (Scrb1) causes severe neural tube defects in the circletail mouse. *Hum Mol Genet*. 2003;12(2):87–98.
29. Zarbalis K, May SR, Shen Y, Ekker M, Rubenstein JL, Peterson AS. A focused and efficient genetic screening strategy in the mouse: identification of mutations that disrupt cortical development. *PLoS Biol*. 2004; 2(8):E219.
30. Fehon RG, McClatchey AI, Bretscher A. Organizing the cell cortex: the role of ERM proteins. *Nat Rev Mol Cell Biol*. 2010;11(4):276–287.
31. Xian W, Schwertfeger KL, Vargo-Gogola T, Rosen JM. Pleiotropic effects of FGFR1 on cell proliferation, survival, and migration in a 3D mammary epithelial cell model. *J Cell Biol*. 2005;171(4):663–673.
32. Bilder D, Perrimon N. Localization of apical epithelial determinants by the basolateral PDZ protein Scribble. *Nature*. 2000;403(6770):676–680.
33. Bilder D. Epithelial polarity and proliferation control: links from the Drosophila neoplastic tumor suppressors. *Genes Dev*. 2004;18(16):1909–1925.
34. Bilder D, Schober M, Perrimon N. Integrated activity of PDZ protein complexes regulates epithelial polarity. *Nat Cell Biol*. 2003;5(1):53–58.
35. Marais R, Wynne J, Treisman R. The SRF accessory protein Elk-1 contains a growth factor-regulated transcriptional activation domain. *Cell*. 1993; 73(2):381–393.
36. Jin C, McKeehan K, Wang F. Transgenic mouse with high Cre recombinase activity in all prostate lobes, seminal vesicle, and ductus deferens. *Prostate*. 2003;57(2):160–164.
37. Soriano P. Generalized lacZ expression with the ROSA26 Cre reporter strain. *Nat Genet*. 1999; 21(1):70–71.
38. Pagliarini RA, Xu T. A genetic screen in Drosophila for metastatic behavior. *Science*. 2003; 302(5648):1227–1231
39. Taylor BS, et al. Integrative genomic profiling of human prostate cancer. *Cancer Cell*. 2010;18(1):11–22.
40. Gioeli D, Mandell JW, Petroni GR, Frierson HF Jr, Weber MJ. Activation of mitogen-activated protein kinase associated with prostate cancer progression. *Cancer Res*. 1999;59(2):279–284.
41. Pearson HB, Phesse TJ, Clarke AR. K-ras and Wnt signaling synergize to accelerate prostate tumorigenesis in the mouse. *Cancer Res*. 2009;69(1):94–101.
42. Scherl A, Li JF, Cardiff RD, Schreiber-Agus N. Prostatic intraepithelial neoplasia and intestinal metaplasia in prostates of probasin-RAS transgenic mice. *Prostate*. 2004;59(4):448–459.
43. Whitmarsh AJ, Yang SH, Su MS, Sharrocks AD, Davis RJ. Role of p38 and JNK mitogen-activated protein kinases in the activation of ternary complex factors. *Mol Cell Biol*. 1997;17(5):2360–2371.
44. Fleischmann A, et al. Immunological microenvironment in prostate cancer: high mast cell densities are associated with favorable tumor characteristics and good prognosis. *Prostate*. 2009;69(9):976–981.
45. Nagasaka K, et al. Human homolog of Drosophila tumor suppressor Scribble negatively regulates cell-cycle progression from G1 to S phase by localizing at the basolateral membrane in epithelial cells. *Cancer Sci*. 2006;97(11):1217–1225.
46. Zeniou-Meyer M, et al. The Coffin-Lowry syndrome-associated protein RSK2 is implicated in calcium-regulated exocytosis through the regulation of PLD1. *Proc Natl Acad Sci U S A*. 2008;105(24):8434–8439.
47. Yin G, Haendeler J, Yan C, Berk BC. GIT1 functions as a scaffold for MEK1-extracellular signal-regulated kinase 1 and 2 activation by angiotensin II and epidermal growth factor. *Mol Cell Biol*. 2004; 24(2):875–885.
48. Audebert S, et al. Mammalian Scribble forms a tight complex with the betaPIX exchange factor. *Curr Biol*. 2004;14(11):987–995.
49. Witte JS. Multiple prostate cancer risk variants on 8q24. *Nat Genet*. 2007;39(5):579–580.
50. Su AI, et al. Molecular classification of human carcinomas by use of gene expression signatures. *Cancer Res*. 2001;61(20):7388–7393.
51. Jackson EL, et al. Analysis of lung tumor initiation and progression using conditional expression of oncogenic K-ras. *Genes Dev*. 2001;15(24):3243–3248.
52. Shappell SB, et al. Prostate pathology of genetically engineered mice: definitions and classification. The consensus report from the Bar Harbor meeting of the Mouse Models of Human Cancer Consortium Prostate Pathology Committee. *Cancer Res*. 2004; 64(6):2270–2305.
53. Kinkade CW, et al. Targeting AKT/mTOR and ERK MAPK signaling inhibits hormone-refractory prostate cancer in a preclinical mouse model. *J Clin Invest*. 2008;118(9):3051–3064.
54. Pearson H, McCarthy A, Collins C, Ashworth A, Clarke A. Lkb1 deficiency causes prostate neoplasia in the mouse. *Cancer Res*. 2008;68(7):2223–2232.
55. Dow LE, et al. The tumour-suppressor Scribble dictates cell polarity during directed epithelial migration: regulation of Rho GTPase recruitment to the leading edge. *Oncogene*. 2007;26(16):2272–2282.
56. Livak KJ, Schmittgen TD. Analysis of relative gene expression data using real-time quantitative PCR and the 2(-Delta Delta C(T)) Method. *Methods*. 2001; 25(4):402–408.
57. Bubendorf L, et al. Survey of gene amplifications during prostate cancer progression by high-throughout fluorescence in situ hybridization on tissue microarrays. *Cancer Res*. 1999;59(4):803–806.
58. El Gammal AT, et al. Chromosome 8p deletions and 8q gains are associated with tumor progression and poor prognosis in prostate cancer. *Clin Cancer Res*. 2010;16(1):56–64.